Ultracompact and unidirectional metallic antennas

Nicolas Bonod,[1,*] Alexis Devilez,[1] Brice Rolly,[1] Sebastien Bidault,[2] and Brian Stout[1]
[1]*Institut Fresnel, CNRS UMR 6133, Ecole Centrale Marseille, Aix-Marseille Université, Domaine Universitaire de Saint Jérôme, 13397 Marseille, France*
[2]*Institut Langevin, CNRS UMR 7587, ESPCI ParisTech, 10 rue Vauquelin, 75231 Paris Cedex 05, France*
(Received 8 June 2010; published 16 September 2010)

We investigate the angular redistribution of light radiated by a single emitter located in the vicinity of dipolar silver nanoparticles. We point out the fundamental role of the phase differences introduced by the optical path difference between the emitter and the particle and demonstrate that the polarizability of the metallic nanoparticle alone cannot predict the emission directionality. In particular, we show that collective or reflective properties of single nanoparticles can be controlled by tuning the distance of a single emitter at a $\lambda/30$ scale. These results enable us to design unidirectional and ultracompact nanoantennas composed of just two coupled nanoparticles separated by a distance achievable with biological linkers.

DOI: 10.1103/PhysRevB.82.115429 PACS number(s): 78.20.Bh, 73.20.Mf, 78.67.−n, 32.50.+d

I. INTRODUCTION

Metallic nanostructures are key elements in the control of light interaction with quantum emitters. They can both focus light in tiny volumes and enhance the radiative decay rates of nearby emitters.[1–9] The latter property has been thoroughly studied in the case of a single emitter coupled to a single nanoparticle.[10–20] It has been shown that the radiative decay rates depend strongly on the distance between the emitter and the nanoparticle. Furthermore, at very short distances from the surfaces (a few nanometers), nonradiative decay channels dominate and the quantum efficiency drops. The coupling efficiency between emitters and optical antennas also depends on the orientation of the dipolar source with respect to the dipolar modes supported by the metallic particles. A longitudinal-coupling geometry significantly enhances the emission decay rates while a transverse interaction leads to moderate enhancements.[19–22]

More recently, the ability of nanoantennas to control the angular emission of single molecules has been investigated.[23–25] This possibility is particularly important since a high directivity facilitates both the excitation of a quantum emitter by a collimated beam as well as the collection of the radiated light.[26] Yagi-Uda antennas have been successfully introduced at optical frequencies[27,28] and their high angular directivity has recently been confirmed experimentally.[29] This antenna geometry combines a director element generally consisting of a finite chain of identical particles and a reflector element typically based on a slightly larger particle.[30,31] A dipolar emitter can be coupled longitudinally to the antenna by utilizing a nanoparticle located near the reflector element.[32] In this configuration, the emitter is off-axis. For an on-axis emitter, the weak transverse coupling with the chain of particles can be reinforced by employing the so-called "super emitter"consisting of a dimer of nanoparticles perpendicular to chain axis.[12,31] Pakizeh and Kall[32] have recently proposed an ultracompact antenna made of two identical metallic particles. The dipolar emitter is then coupled to a dark mode characterized by opposite phase dipolar modes induced in the two neighboring particles. In that case, it has been shown that the emitter radiates predominantly in only one half space and can thus be characterized as unidirectional.

This paper is dedicated to studying how nearby spherical nanoparticles modify the angular distribution of light emitted by an oscillating dipole. In particular, we provide a thorough study of the phase differences between the dipolar source and the dipolar mode induced in the particle. We emphasize that these phase differences must take into account the optical path between the emitter and the particle in addition to the polarizability of the particle. We show that by tuning the position of a single emitter from a single nanoparticle by a few tens of nanometers, we can sufficiently modify the dephasing to control the reflective or collective properties of the particle at a given frequency. When the phase difference between the exciting and induced dipoles is strictly equal to π, an equal part of the energy is radiated into each of the half spaces surrounding the emitter (the separation plane being perpendicular to the axis containing the dipoles). We then apply these results to the design of highly unidirectional antennas composed of two nanospheres separated by a mere 50 or 60 nm. The basic concept is similar to the idea underlying the design of Yagi-Uda optical antennas, which associate the collective and reflective properties of nanoparticles[27,28] but at much smaller interparticle distances and in simpler geometries. Taking into account the phase lag induced by the distance between the emitter and the nanoparticle, highly directional antennas can be designed with only two nanoparticles. We will first emphasize the role of the distance between the emitter and the nanoparticles by designing a directional antenna composed of identical particles, i.e., with strictly identical polarizabilities. Furthermore, by tuning the relative size of the two particles, it is possible to design an antenna smaller than $\lambda/2$ that channels light radiated by a single emitter in the angular aperture of commercial microscope objectives.[33]

II. RADIATION PROPERTIES OF A DIPOLAR EMITTER COUPLED TO A SINGLE NANOPARTICLE

We first investigate the radiation pattern of a single emitter located near a single 90 nm silver particle. The dipolar

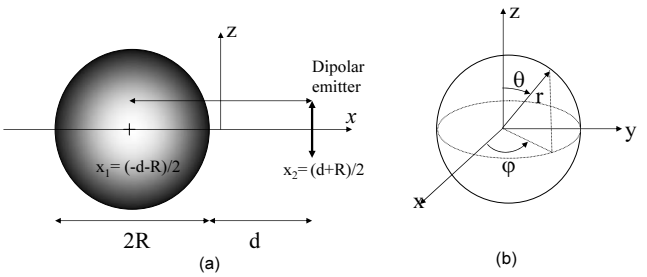

FIG. 1. (a) Sketch of a dipolar emitter oriented along the z axis and located at a distance d from the surface of a silver nanosphere. The refractive index of silver is taken from Ref. 37. Silver nanospheres are embedded in a polymer of refractive index 1.5. (b) The spherical coordinates used in the analytical expressions.

emitter is polarized along the z axis in order to provide a transverse coupling with the nanoparticle as sketched in Fig. 1. The emission properties of the dipolar emitter are calculated in the framework of rigorous Lorentz-Mie theory and combined with multiple scattering theory in configurations where more than one silver particle is present.[34–36] This analytical method is particularly well suited to tackle light scattering by an ensemble of nanospheres. In order to ensure an accurate modeling of the short-range couplings, the calculations presented in this study are carried out with 30 multipole orders. Nevertheless, let us emphasize that the electromagnetic response of the metallic particles under consideration is predominately dipolar in nature, resulting in a rapid multipole convergence. Consequently, a dipole approximation (first order) would qualitatively exhibit all the underlying physics observed in this work.

The radiation patterns are obtained from the radial component of the Poynting vector in the far field. In order to estimate how much light is collected or reflected by the metallic particle, we define the reflection coefficient R as the ratio of the power emitted in the $x \geq 0$ hemisphere with respect to the total radiated power.

In this work, we pay particular attention to the dephasing between the emitting and induced dipoles. When the dipole approximation dominates (as it does here), it is sufficient to calculate the electric field at the center of the metallic particle. The induced dipole moment of the nanoparticle is then obtained by multiplying the total electric field by $V_s \epsilon_0 (\varepsilon_s - \varepsilon_b)$ where V_s is the volume of the sphere, ϵ_0 the permittivity of vacuum and ε_s and ε_b are the relative permittivities of the metal and the background media, respectively. For small particles, the quasistatic approximation applies and we can express the resulting phase differences as the sum of the phase differences due to the optical path difference from the emitter and the polarizability of the particle. It must be stressed that in previous works, attention was focused on the phase difference of a nanoparticle polarizability with respect to its local excitation fields while in this work we emphasize importance of taking into account the additional phase difference induced by the (small but non-negligible) optical path between the emitter and the nanoparticle. We point out that we chose the common convention of the phase differences defined to lie in the range from $-\pi$ to π.

The phase differences $\Delta\phi$ between the emitter and dipole moment of a (D=90 nm) silver nanoparticle are displayed in

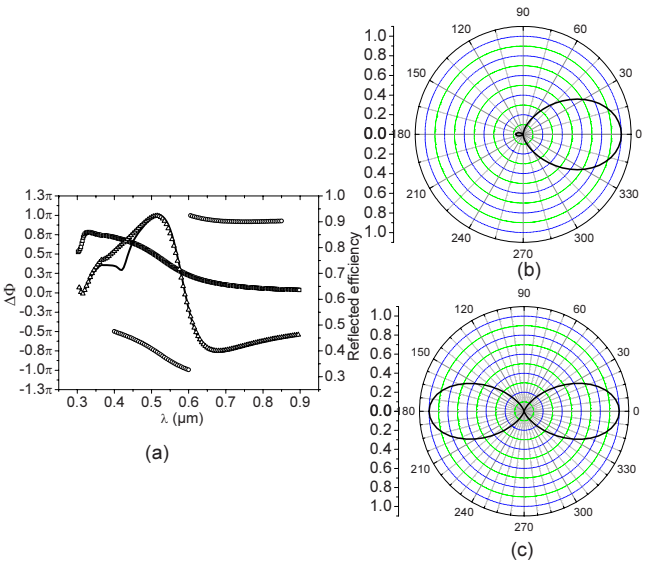

FIG. 2. (Color online) (a) A dipolar emitter oriented along the z axis is located at a distance d=30 nm from a silver sphere of diameter 90 nm. The phase difference between the emitting and induced dipoles (circles, left scale) and reflection efficiency (right scale: full line: complete calculation, triangles: dipolar approximation) as a function of the emission wavelength. Emission patterns of the oscillating dipole at (b) λ=510 nm and (c) λ=600 nm in the xOz plane, (d=30 nm) calculated by plotting the radial component of the Poynting vector normalized by the forward emitted value as a function of the polar angle.

Fig. 2 (circles) as a function of the emission wavelength. The emitting and induced dipoles are precisely in opposing phase at λ_r=600 nm, $\Delta\phi=\pi$, and remain roughly in opposite phase for longer wavelengths. For wavelengths smaller than λ_r=600 nm, $\Delta\phi$ varies as a function of λ, and the induced dipole is generally out-of-phase with respect to the emitter. The phase of the polarizability of the nanoparticle is also displayed (squares) and the phase value of $\pi/2$ at λ =500 nm indicates the plasmon resonance. Let us now investigate the radiation properties of the coupled system in terms of the reflection efficiency of the nanosphere. We present in Fig. 2 the reflection efficiency, R, of the nanoparticle (i.e., defined as the power emitted in the $x \geq 0$ half space over the total emitted power) as a function of the emission wavelength λ. When the reflection efficiency is lower than 0.5, the dipole preferentially radiates toward the $x \leq 0$ half space and the nanoparticle behaves as a collector (cf. Fig. 1: the nanoparticle is located on the negative x axis). The full line in Fig. 2 clearly indicates that depending on the phase differences between the emitting and induced dipoles, a metallic nanoparticle can either collect or reflect light radiated by a single emitter. Let us mention that the dipolar approximation (triangles) exhibits almost all the features of the radiation properties, meaning that the coupling between the single emitter and the metallic particle is almost perfectly dipolar for λ > 450 nm. For wavelengths $\lambda > \lambda_r$, the emitting and induced dipoles are nearly opposite in phase and the emitter radiates preferentially toward the metallic nanoparticle with R dropping down to 0.4 at λ=665 nm. For $\lambda < \lambda_r$, the emitting and induced dipoles are out-of-phase and

the nanoparticle reflects with a rather high efficiency the radiated light since R reaches 90% at $\lambda=510$ nm.

The emission pattern of the light radiated by the exciting dipole at $\lambda=510$ nm is reconstructed in Fig. 2(b) by plotting the radial component of the Poynting vector normalized by the forward emission value as a function of the polar angle (in the plane xOz). This result demonstrates the good unidirectionality offered by a single nanoparticle. The angular width of the emission pattern defined as the angle between the on-axis maximum value and the direction of half maximum value is on the order of $\pm 40°$. Finally, it is interesting to note that for $\lambda=\lambda_r$, the ratio of the radiated energy in both half spaces is precisely equal to 1. It may seem surprising that a highly asymmetric environment (a single particle at the left of the emitter) results in perfectly symmetric radiation [see the radiation pattern in Fig. 2(c)]. To fully understand this counter-intuitive result, let us consider the analytic expression of the emission of two dipoles with moments denoted $\mathbf{p}_1$ and $\mathbf{p}_2$. They are placed along the x axis with separation $d+a$, and oriented along the z axis [see Fig. 1(a)]. Let us note $x_1=-(d+a)/2$ and $x_2=(d+a)/2$ the positions of the dipoles along the x axis. We consider that in the far-field limit ($r \gg \lambda$),

$$\begin{aligned}|\mathbf{r}-\mathbf{x}_j|-r &= \sqrt{(x-x_j)^2+y^2+z^2}-r \\ &\approx r(\sqrt{1-2xx_j/r^2}-1) \\ &\approx -x_j(x/r) \approx -x_j \sin(\theta)\cos(\varphi).\end{aligned}$$

The electric and magnetic fields produced in the far field by $\mathbf{p}_1$ ($j=1$) and $\mathbf{p}_2$ ($j=2$) then write

$$\mathbf{E}_j(r,\theta,\varphi) = \left(\frac{\omega}{c}\right)^2 \frac{1}{4\pi r\epsilon_0} e^{ik|\mathbf{r}-\mathbf{x}_j|}[(\mathbf{e}_r \times \mathbf{p}_j)\times \mathbf{e}_r] \quad (1)$$

$$= \left(\frac{\omega}{c}\right)^2 \frac{1}{4\pi r\epsilon_0} e^{ikr} e^{-ikx_j \sin(\theta)\cos(\varphi)} p_j \sin(\theta)(-\mathbf{e}_\theta), \quad (2)$$

$$\mathbf{H}_j(r,\theta,\varphi) = \frac{k\omega}{4\pi r} e^{ikr} e^{-ikx_j \sin(\theta)\cos(\varphi)} p_j \sin(\theta)(-\mathbf{e}_\varphi) \quad (3)$$

with $\mathbf{e}_r$, $\mathbf{e}_\theta$, and $\mathbf{e}_\varphi$ the unit vectors of the spherical basis [Fig. 1(b)]. The resulting far-field, time-averaged Poynting vector of the sum of these fields writes

$$\mathbf{P}(r,\theta,\varphi) = \frac{1}{2}\mathrm{Re}[(\mathbf{E}_1+\mathbf{E}_2)^* \times (\mathbf{H}_1+\mathbf{H}_2)] \quad (4)$$

$$\begin{aligned}&= \frac{\omega^3 k}{32\pi^2\epsilon_0 c^2 r^2}(p_1^* e^{-ikr} e^{ikx_1 \sin(\theta)\cos(\varphi)} + p_2^* e^{-ikr} e^{ikx_2 \sin(\theta)\cos(\varphi)}) \\ &\times (p_1 e^{ikr} e^{-ikx_1 \sin(\theta)\cos(\varphi)} + p_2 e^{ikr} e^{-ikx_2 \sin(\theta)\cos(\varphi)}) \\ &\times \sin^2(\theta)\mathbf{e}_r \end{aligned} \quad (5)$$

$$\begin{aligned}&= \frac{\omega^3 k}{32\pi^2\epsilon_0 c^2 r^2}[|p_1|^2 + |p_2|^2 \\ &+ 2\,\mathrm{Re}(p_1 p_2^* e^{ik(d+a)\sin(\theta)\cos(\varphi)})]\sin^2(\theta)\mathbf{e}_r. \end{aligned} \quad (6)$$

To study the symmetry of the radiation pattern, we compute the sum of the Poynting vectors in one direction and in the opposite direction

$$\Delta\mathbf{P}(r,\theta,\varphi) = \mathbf{P}(r,\theta,\varphi) + \mathbf{P}(r,\pi-\theta,\varphi+\pi) \quad (7)$$

$$= \frac{\omega^3 k}{16\pi^2\epsilon_0 c^2 r^2}\mathrm{Re}\{2ip_1 p_2^* \sin[k(d+a)\sin(\theta)\cos(\varphi)]\}\sin^2(\theta)\mathbf{e}_r. \quad (8)$$

In our case, we are interested by the evolution of $\Delta\mathbf{P}$ with respect to the relative phase $\phi=\phi_1-\phi_2$ between $p_1=|p_1|e^{i\phi_1}$ and $p_2=|p_2|e^{i\phi_2}$:

$$\begin{aligned}\Delta\mathbf{P}(r,\theta,\varphi) = \frac{\omega^3 k}{16\pi^2\epsilon_0 c^2 r^2}&\{-2|p_1||p_2|\sin(\phi) \\ &\times \sin[k(d+a)\sin(\theta)\cos(\varphi)]\}\sin^2(\theta)\mathbf{e}_r. \end{aligned} \quad (9)$$

Hence when $\phi=k\pi$ with $k \in \mathbf{N}$, $\Delta\mathbf{P}=0$ for any value of the dipolar amplitudes $|p_1|$ and $|p_2|$. This calculation demonstrates that when the emitted and induced dipoles are in phase or in opposite phase, the emission from the two dipoles is perfectly symmetric with respect to the origin while the electromagnetic environment of the emitter can be highly asymmetric. This confirms that the wavelength of the plasmonic resonance ($\lambda=500$ nm) taken alone cannot predict the directionality of the emission and that the distance between the emitter and the nanoparticle plays a crucial role. Moreover, this model exhibits a very interesting property: in a given direction defined by θ and ϕ, the change in the sign of $\sin(\phi)$ will change the sign of $\Delta\mathbf{P}$, for every distance d. In order to confirm this assumption, phase differences [Fig. 3(a)] and reflection ratios [Fig. 3(b)] are now displayed as a

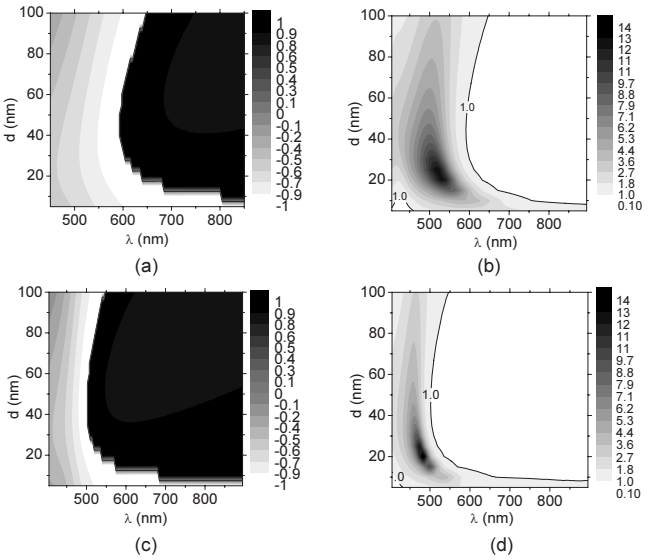

FIG. 3. (a) Phase differences normalized by π between the dipolar emitter and the induced dipolar moment of the nanoparticle and (b) reflection ratio defined as the ratio of the power emitted toward the right and left half spaces respectively as a function of the wavelength of emission and the distance d between the emitter and the metallic surface of a 90 nm silver sphere. (c) and (d) show similar results as (a) and (b), respectively, but for a 60 nm sphere.

function of distance d and λ.

These graphs confirm the clear correlation between reflection efficiency and the phase differences of the emitting and induced dipoles. The isoefficiency line is plotted in Fig. 3(b) when the directionality is null and it matches the isodephasing line [see Fig. 3(a)] plotted for $\Delta\phi=\pi$. Calculations performed for a 60 nm silver particle [Figs. 3(c) and 3(d)] show that a similar behavior is obtained but that the opposite-phase wavelength, λ_r, is shifted toward shorter wavelengths. These graphs evidence that in the 500–600 nm range (with d =30 nm), the smaller particles (60 nm) mostly collect electromagnetic radiation while larger particles (90 nm) act as reflectors. This property allows the design of Yagi-Uda antennas with a reflector made of slightly larger particles and a collector made of an array of identical smaller particles.[27–31] More importantly, these calculations show that at a given frequency, a single sphere can act as a reflector or a collector depending on its distance from the emitter, and that this behavior can be controlled inside a very small range of distances (a few tens of nanometer_S_). For example, we can observe in Fig. 3(d) that at $\lambda=550$ nm, the nanoparticle behaves as a collector when it is at a distance of 40 nm from the emitter while it behaves as a reflector when this distance is reduced to 10 nm. Consequently, it is possible to design unidirectional antennas by assembling two identical particles, i.e., with identical polarizabilities and by tuning the distances between the emitter and both particles. However, Fig. 3 suggests that a stronger directionality can be achieved by assembling two particles of different diameters with minimum and maximum reflection efficiencies at the emission wavelength, a property that cannot be achieved with equal diameters. We can thus design an ultracompact antenna made of 90 and 60 nm particles at an equal 30 nm distance from the emitter, geometry chosen to optimize the dephasing between the dipolar moments of the nanospheres and the emitter.

III. ULTRACOMPACT AND UNIDIRECTIONAL NANOANTENNA

Before discussing antennas with nonequal diameters, let us begin this section by designing an ultracompact antenna composed of two identical nanoparticles of diameters 60 nm closely separated by a distance of only 50 nm. The emitter is located at 10 nm from the first particle (which thus acts as the reflector) and 40 nm from the second particle (the collector) [see Fig. 4(a)]. Figure 4(b) shows the reflection efficiency as a function of the wavelength of emission. A good directivity can thus be achieved with strictly identical particles since 70% of the emitted energy is radiated into the positive x half space. Let us note that both distances, respectively, 10 nm and 40 nm are much smaller than the emitting wavelength and achievable with biological linkers.[7,18]

Let us now design an asymmetric antenna made of two silver particles with different diameters to optimize their reflective and collective properties. The antenna, consisting of 60 and 90 nm diameter silver spheres, was optimized with respect to the particle sizes while keeping d equal to 30 nm [see Fig. 5(a)]. In a first step, we compute the phase differences between the emitter and the two induced dipolar modes supported by the particles. The wavelength range in which one particle acts as a collector while the other reflects radiation exceeds 100 nm, which is larger than the width of a typical fluorescent emitter. Figure 5(b) shows that this antenna geometry fulfills these conditions for wavelengths ranging from 475 to 600 nm. As expected, the ratio of the radiated power toward the $x\geq 0$ half space is maximum

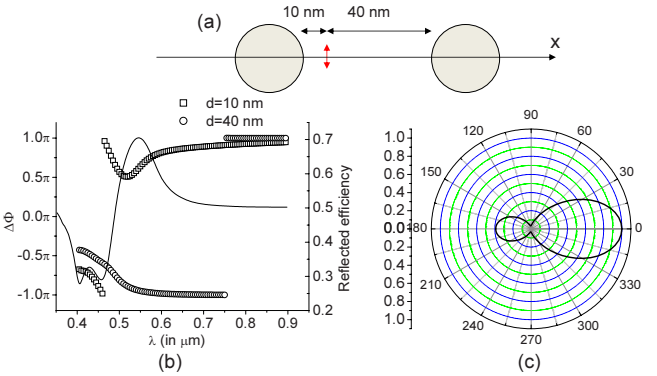

FIG. 4. (Color online) (a) The nanoantenna is composed of two identical silver nanoparticles of diameter 60 nm. The emitter is located at 10 nm from the left particle, and at 40 nm from the right particle. (b) Full line, right scale: reflection efficiency as a function of the emitted wavelength; circles and squares, left scale: dephasing of the emitting and induced dipoles supported by the 60nm sphere for 40nm (circles) and 10nm (squares) spacings. (c) Emission pattern of the oscillating dipole at $\lambda=550$ nm in the xOz plane.

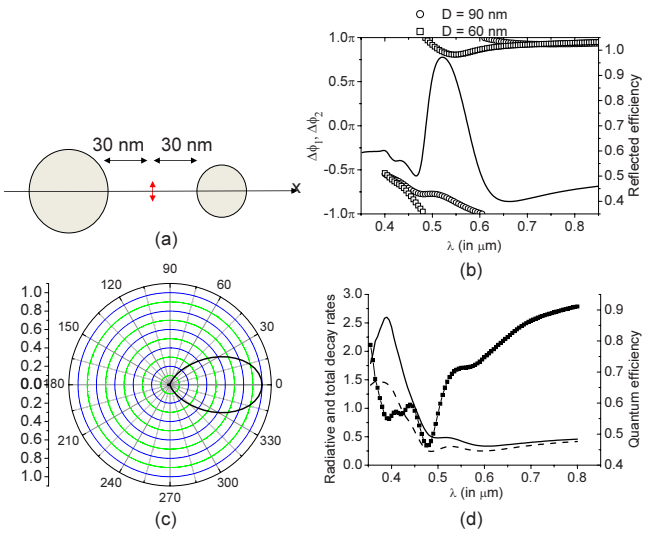

FIG. 5. (Color online) (a) The nanoantenna is composed of silver particles of diameter 60 and 90 nm. The emitter is located at 30 nm from both particles. (b) Full line, right scale: reflection efficiency as a function of the emitted wavelength; circles and squares left scale: dephasing of the emitting and induced dipoles supported by spheres of diameter 90 nm (circles) and 60 nm (squares). (c) Emission pattern of the oscillating dipole at $\lambda=550$ nm in the xOz plane. (d) Full and circles, left scale: radiative (dashed lines) and total (full line) decay rates enhancements as a function of the wavelength emission. Full line+squares, right scale: quantum efficiency (the intrinsic quantum efficiency is equal to 1).

when the phases are of opposite sign, and it can reach more than 97% at $\lambda=520$ nm. The emission pattern is reconstructed in Fig. 5(c) at $\lambda=520$ nm as a function of the polar angle (in the plane xOz). It confirms the high unidirectionality of this antenna since the emitted power toward the left half plane is unobservable at this scale. Moreover, this antenna narrows the angular redistribution of emitted light compared to a single nanoparticle since the angular width of the emission cone is less than $\pm 30°$. Such angular openings are easily achievable with commercial microscope objectives.[33] In practice, this asymmetric nanoantenna, although much smaller than the vacuum emission wavelength of the oscillating dipole, is almost perfectly unidirectional.

For the sake of completeness, the evolution of the radiative and total decay rates and the quantum efficiency of the emitter in the vicinity of the optical antenna are displayed in Fig. 5(d). For that purpose, the total emitted power, P_{tot}, and the radiated power, P, are calculated by integrating the radial component of the Poynting vector over a spherical surface surrounding the source, at respective distances of 1 nm and 50 μm. The total (Γ_{tot}) and radiative (Γ_{rad}) decay rate enhancements are then obtained by normalizing the emitted power in the presence of the antenna by the emitted power (P_0) in the homogeneous background medium: $\Gamma_{\mathrm{tot}}=P_{\mathrm{tot}}/P_0$ and $\Gamma_{\mathrm{rad}}=P_{\mathrm{rad}}/P_0$. The quantum efficiency is then defined as $\eta=\Gamma_{\mathrm{rad}}/(\Gamma_{\mathrm{tot}}+(1-\eta_i)/\eta_i)$ where η_i is the intrinsic quantum efficiency. We consider in this work a perfect emitter ($\eta_i=1$). Figure 5(d) shows that the high directionality achieved at $\lambda=520$ nm is not associated with a drop of the radiative decay rates which confirms that it relies on the association of the reflective and collective features of nanoparticles rather than on opposing phases between the induced dipoles of the nanoparticles.[32] The radiative decay rates obtained are comparable with those observed when dealing with Yagi-Uda antennas[30,31] and they are significantly enhanced by coupling the source dipole to a "superemitter" as shown in Fig. 6(a). In this last case, we consider a more complex antenna geometry to combine unidirectionality and strong radiative rate enhancements by introducing two dipolar particles coupled longitudinally to the emitter. Figure 6(b) shows that a super emitter can strongly enhance the radiative decay rates by up to 3 orders of magnitude. In particular, at $\lambda=610$ nm, the quantum yield is maximum, the radiative decay rate is enhanced by more than 500 and the unidirectionality is preserved as shown on Fig. 6(d).

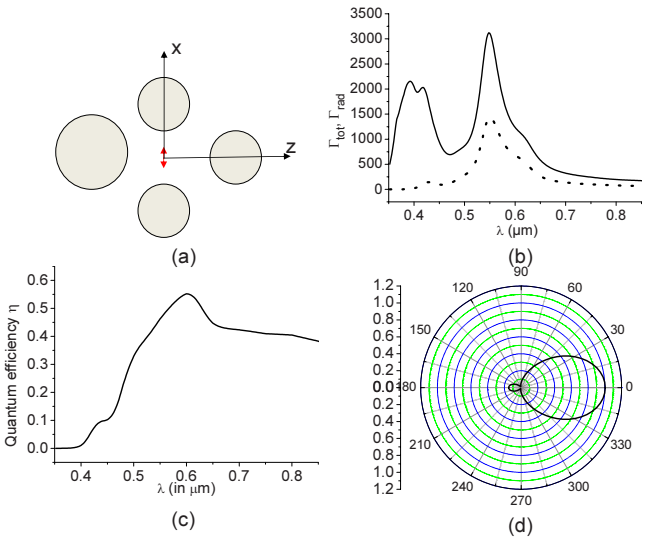

FIG. 6. (Color online) (a) Sketch of the ultracompact nanoantenna+super emitter: the dipolar source is longitudinally coupled with two 60 nm silver particles on the z axis, with an emitter-particle distance of 8 nm. The emitter-particle distances on the x axis are equal to Fig. 5(a) at 30 nm. (b) Radiative and total decay rate enhancements as a function of the emission wavelength. (c) Quantum efficiency as a function of the emission wavelength. (d) Emission pattern of the oscillating dipole at $\lambda=610$ nm in the xOz plane.

IV. CONCLUSION

The reflection or collection behavior of the nanoparticle depends on the total phase difference between the emitting and induced dipoles which includes both the polarizability of the metallic particle and the optical path between the emitter and the nanoparticle. We showed the importance of the role of the optical path between the emitter and a metallic particle on the redistribution of light for distances smaller than $\lambda/30$. One consequence of this observation was to remark that when the emitting and induced dipoles are exactly in opposing phase, the ratio between the radiated powers in the backward and forward directions is precisely equal to unity. We unveiled the importance of the optical path by designing a directional antenna composed of two identical nanoparticles. The reflective and collective properties were tuned by controlling the distance between the emitter and the nanoparticles at a scale of $\lambda/30$. We also presented a means to design highly directive and ultracompact nanoantennas by tuning the relative sizes of the silver particles (while still keeping the overall size much smaller than the vacuum emission wavelength). While angular openings obtained with single particles are around 40°, the dimer nanoantennas narrow the angular opening of emitted radiation to around 30°, rendering the radiation readily collectible by commercial microscope objectives. Finally, we showed that the radiative decay rate of an emitter can be increased by three orders of magnitude by introducing a dimer antenna longitudinally coupled to the emitter while preserving a high directivity.

*nicolas.bonod@fresnel.fr

[1] H. Metiu, Prog. Surf. Sci. **17**, 153 (1984).
[2] D. Gérard, J. Wenger, N. Bonod, E. Popov, H. Rigneault, F. Mahdavi, S. Blair, J. Dintinger, and T. W. Ebbesen, Phys. Rev. B **77**, 045413 (2008).
[3] N. Bonod, E. Popov, D. Gerard, J. Wenger, and H. Rigneault, Opt. Express **16**, 2276 (2008).
[4] H. Tamaru, H. Kuwata, H. T. Miyazaki, and K. Miyano, Appl. Phys. Lett. **80**, 1826 (2002).
[5] W. Rechberger, A. Hohenau, A. Leitner, J. R. Krenn, B. Lamprecht, and F. R. Aussenegg, Opt. Commun. **220**, 137 (2003).
[6] K. Li, M. I. Stockman, and D. J. Bergman, Phys. Rev. Lett. **91**, 227402 (2003).
[7] S. Bidault, F. J. García de Abajo, and A. Polman, J. Am. Chem. Soc. **130**, 2750 (2008).
[8] A. Kinkhabwala, Z. Yu, S. Fan, Y. Avlasevich, K. Mullen, and W. E. Moerner, Nat. Photonics **3**, 654 (2009).
[9] J.-W. Liaw, J.-S. Chen, and J.-H. Chen, J. Quant. Spectrosc. Radiat. Transf. **111**, 454 (2010).
[10] J. Gersten and A. Nitzan, J. Chem. Phys. **75**, 1139 (1981).
[11] R. Ruppin, J. Chem. Phys. **76**, 1681 (1982).
[12] J. N. Farahani, D. W. Pohl, H.-J. Eisler, and B. Hecht, Phys. Rev. Lett. **95**, 017402 (2005).
[13] P. Anger, P. Bharadwaj, and L. Novotny, Phys. Rev. Lett. **96**, 113002 (2006).
[14] S. Kühn, U. Håkanson, L. Rogobete, and V. Sandoghdar, Phys. Rev. Lett. **97**, 017402 (2006).
[15] R. Carminati, J.-J. Greffet, C. Henkel, and J. M. Vigoureux, Opt. Commun. **261**, 368 (2006).
[16] L. Rogobete, F. Kaminski, M. Agio, and V. Sandoghdar, Opt. Lett. **32**, 1623 (2007).
[17] Y. Chen, K. Munechika, and D. S. Ginger, Nano Lett. **7**, 690 (2007).
[18] J. Seelig, K. Leslie, A. Renn, S. Kuhn, V. Jacobsen, M. van de Corput, C. Wyman, and V. Sandoghdar, Nano Lett. **7**, 685 (2007).
[19] H. Mertens, A. F. Koenderink, and A. Polman, Phys. Rev. B **76**, 115123 (2007).
[20] G. Colas des Francs, A. Bouhelier, E. Finot, J. C. Weeber, A. Dereux, C. Girard, and E. Dujardin, Opt. Express **16**, 17654 (2008).
[21] C. Vandenbem, D. Brayer, L. S. Froufe-Perez, and R. Carminati, Phys. Rev. B **81**, 085444 (2010).
[22] M. Ringler, A. Schwemer, M. Wunderlich, A. Nichtl, K. Kurzinger, T. A. Klar, and J. Feldmann, Phys. Rev. Lett. **100**, 203002 (2008).
[23] H. Gersen, M. F. Garcia-Parajo, L. Novotny, J. A. Veerman, L. Kuipers, and N. F. van Hulst, Phys. Rev. Lett. **85**, 5312 (2000).
[24] S. Kühn, G. Mori, M. Agio, and V. Sandoghdar, Mol. Phys. **106**, 893 (2008).
[25] T. H. Taminiau, F. D. Stefani, F. B. Segerink, and N. F. van Hulst, Nat. Photonics **2**, 234 (2008).
[26] A. Devilez, B. Stout, and N. Bonod, ACS Nano **4**, 3390 (2010).
[27] J. Li, A. Salandrino, and N. Engheta, Phys. Rev. B **76**, 245403 (2007).
[28] H. F. Hofmann, T. Kosako, and Y. Kadoya, New J. Phys. **9**, 217 (2007).
[29] T. Kosako, Y. Kadoya, and H. F. Hofmann, Nat. Photonics **4**, 312 (2010).
[30] T. H. Taminiau, F. D. Stefani, and N. F. van Hulst, Opt. Express **16**, 10858 (2008).
[31] A. F. Koenderink, Nano Lett. **9**, 4228 (2009).
[32] T. Pakizeh and M. Kall, Nano Lett. **9**, 2343 (2009).
[33] C. Huang, A. Bouhelier, G. C. des Francs, A. Bruyant, A. Guenot, E. Finot, J. C. Weeber, and A. Dereux, Phys. Rev. B **78**, 155407 (2008).
[34] B. Stout, J. C. Auger, and A. Devilez, J. Opt. Soc. Am. A **25**, 2549 (2008).
[35] M. Lax, Rev. Mod. Phys. **23**, 287 (1951).
[36] W. J. Wiscombe, Appl. Opt. **19**, 1505 (1980).
[37] E. D. Palik, in *Handbook of Optical Constants of Solids*, edited by E. D. Palik (Academic Press, New York, 1985).